JOURNAL OF MATERIALS SCIENCE **39** (2004) 3985–3998

# Metastable microstructures in rapidly solidified zirconium alloys

S. BANERJEE, G. K. DEY
*Bhabha Atomic Research Centre, Trombay, Mumbai-400 085, India*

Zirconium alloys exhibit a wide variety of phase transformations. The present review outlines some aspects of phase transformations, which are encountered in rapidly solidified zirconium alloys. The possibility of solidification of unalloyed zirconium directly into the low temperature phase is examined and the role that solidification microstructure plays in modifying the $\beta$ to $\alpha$ martensitic transformation in rapidly solidified material is discussed. Zirconium alloys undergo two types of displacive transformations, namely, the martensitic transformation and the $\omega$ transformation. The influence of rapid solidification on the transition from the martensitic to the $\omega$ transformation is also discussed. Addition of transition metals are known to depress the melting point of zirconium alloys very drastically. As a consequence, glass forming abilities of a number of binary and ternary zirconium alloys are quite strong. A number of zirconium based metal-metal amorphous alloys have been synthesized using rapid solidification. In recent years, this work has been extended to bulk metallic glasses, which usually contain a larger number of alloying elements. Crystallization of these glasses and quasi-crystalline phase formation in these systems is also discussed. 

## 1. Introduction

Zirconium based alloys exhibit many interesting phase transformations. In fact the variety of phase transformations that one encounters in zirconium based systems is even wider than that in iron based systems that are often taken as examples for illustrating phase transformations of different kinds in metals, alloys, intermetallics and ceramics. An attempt will be made in a forthcoming publication [1] to demonstrate that zirconium based systems not only provide a wider range of transformations but also reveal some of the fundamental features of transformations in a more lucid manner.

Rapid solidification processing has been employed extensively for controlling phase transformations involving both solidification and subsequent solid state transformations. An investigation on how rapid solidification processing influences transformation behaviour of zirconium based alloys was initiated in 1978 in the Engineering and Applied Sciences Department of University of Sussex under the leadership of Professor Robert W. Cahn. The subject grew since then in different directions and today multicomponent zirconium alloys find an important place amongst the new class of amorphous materials usually known as bulk metallic glasses. The present paper which is dedicated to Professor Robert W. Cahn on the occasion of his 75th birthday deals with some novel phase transformation aspects of rapidly solidified zirconium alloys involving both solidification and solid state transformations.

## 2. Direct liquid to $\alpha$ transformation

The Allotropic modification from the low temperature hcp $\alpha$ to the high temperature [above 862°C] bcc $\beta$ is well known for pure zirconium. Liquid zirconium when solidifying under equilibrium conditions generates the $\beta$ phase, which subsequently transforms into $\alpha$ on further cooling. Under nonequilibrium cooling conditions of rapid solidification processing, there exists a possibility of transforming the liquid directly into the low temperature $\alpha$ phase. The feasibility of such a process can be examined from thermodynamic considerations by plotting free energy [$G$] as a function of temperature [$T$] for the liquid, the $\beta$ and $\alpha$ phases. The $G$-$T$ plots for Zr were drawn from data obtained from ref. 2 and are shown in Fig. 1. The equilibrium melting temperature is given by the point of intersection of the free energy versus temperature lines corresponding to the liquid and the $\beta$ phase. In a similar manner one can argue that there exists a 'melting temperature' [$T_{\alpha/L}$] of the $\alpha$ phase which will be given by the point of intersection of $G$-$T$ lines corresponding to the liquid and the $\alpha$ phases. Therefore, from thermodynamic considerations direct liquid to $\alpha$ transformations is feasible only when a super cooling of the liquid is achieved to a temperature below $T_{\alpha/L}$. In order to examine this possibility, experiments were conducted by rapidly quenching pure zirconium and examining their microstructure with a view towards identifying the transformation path.

Banerjee and Cantor [3] have reported the microstructure produced in unalloyed zirconium and in

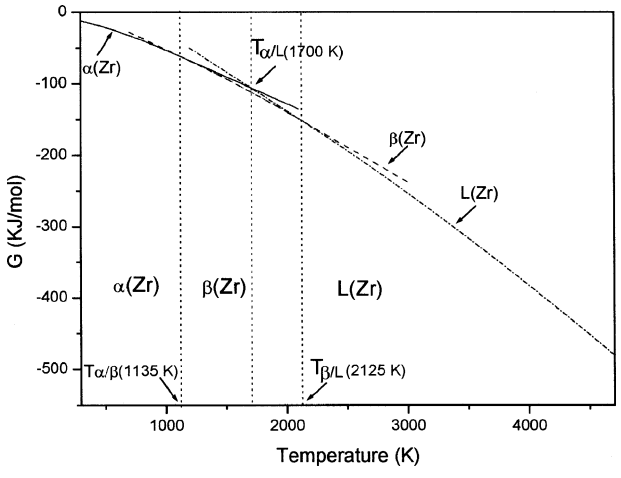


*Figure 1* Free energy ($G$) vs. temperature ($T$) plot for pure Zr. The intersection of the curve for $\alpha$ Zr phase with that of the liquid phase gives the melting point of the $\alpha$ Zr phase.

zirconium-niobium alloys by rapid quenching from the liquid state. In the majority of the experiments, it was seen that the liquid first solidified into the $\beta$ phase, which subsequently underwent $\beta \rightarrow \alpha$ martensitic transformations (Fig. 2a). However, in some experiments it was found that cellular structure of the $\alpha$ phase is produced with intercellular region being rich in Si and O (Fig. 2b). Energy dispersive X-ray analysis of the $\alpha$ cells and intercellular regions revealed that these samples which underwent direct liquid to $\alpha$ transformations were contaminated with oxygen and silicon, both these elements being potent $\alpha$ stabilizers.

This set of experiments, therefore, pointed out that rapid solidification by splat quenching with cooling rate of about $10^{6\circ}$C/s is not able to suppress the nucleation of the $\beta$ phase during solidification in pure zirconium in spite of the large super cooling introduced. However, with the enhancement of $\alpha$ stability, the requirement of super cooling for direct $\alpha$ formation is reduced making it possible to nucleate the $\alpha$ phase directly by skipping the $\beta$ phase altogether. This aspect of direct solidification into a low temperature phase skipping the high temperature equilibrium phase is an issue of fundamental interest that needs to be examined in detail. However, very few studies have been made addressing this issue.

## 3. Influence of rapid solidification on martensitic transformation

Cantor and co-workers [4, 5] have systematically studied the influence of rapid solidification on the martensite microstructure produced in rapidly solidified iron-based alloys. The most important result they have reported is that the size of the martensite plates is substantially reduced by rapid solidification processing. They have rationalized this result in terms of the refinement of the austenite grains emanating from the liquid phase during rapid solidification and the consequent reduction in the size of martensite plates which are confined within the parent austenite grains.

The crystallography of the martensitic transformation in zirconium and its alloys is relatively simple as the Bain strain, which transforms the lattice from the $\beta$ phase to the $\alpha$ phase at 862°C (for pure zirconium), nearly satisfies the invariant plane strain (IPS) condition [6]. This can be seen from the lattice correspondence (Fig. 3a) and the magnitude of lattice (Bain) distortion associated with the transformation, as given by

$$= \begin{matrix} \eta_1 & 0 & 0 \\ 0 & \eta_2 & 0 \\ 0 & 0 & \eta_3 \end{matrix}$$

where, $\eta_1 = \sqrt{3}/2a_\alpha/a_\beta$; $\eta_2 = a_\alpha/a_\beta$ and $\eta_3 = c_\alpha/2a_\beta$. These are the distortions in the principal directions. $a_\alpha$, $c_\alpha$ and $a_\beta$ are the lattice parameters of the $\alpha$ and the $\beta$ phases respectively. The substitution of lattice parameters of pure zirconium shows that the lattice strains are approximately 10% tensile, 10% compressive and 2% tensile, respectively, along $\eta_1$, $\eta_2$ and $\eta_3$ directions. If the 2% tensile strain in the $\eta_3$ direction is neglected, the strain ellipsoid (Fig. 3b) shows that the vectors OA and OX and the vertical planes passing through AOB and X OY remain undistorted by the Bain strain. A rigid body rotation of 5.26° around the $\eta_3$ axis, which brings OA′ in coincidence with OA, when superimposed on the Bain strain establishes the IPS condition. The rigid body rotation can be either clockwise or anticlockwise making the vertical planes passing through OA′ or OX′ as the habit plane, which remains undistorted and unrotated.

In order to accommodate the 2% strain along the $\eta_3$ direction, a lattice invariant strain of a much smaller magnitude, in comparison with that necessary in steels, needs to be introduced. As a consequence, the substructure consisting of either a stack of twins or a periodic array of dislocations, is far less dense in zirconium martensites than in steels and therefore more amenable for detailed characterization. The lattice invariant strain (LIS) systems which are most probable from the consideration of minimization of the LIS magnitude are the following:

(a) Twin along $\{10\bar{2}1\}$ plane
(b) Slip in the $\{10\bar{2}1\}$ $\langle\bar{2}123\rangle$ system
(c) a combination of $\{1\bar{2}1\}$ twin and a $\{10\bar{2}1\}$ $\langle\bar{2}123\rangle$ slip which are mutually compatible.

Experimental validation of all these modes of LIS and of the corresponding habit planes has clearly vindicated the applicability of the phenomenological theory in this system. The large spacing of internal twins has also enabled creation of a zig-zag habit in a scale easily resolvable by TEM. The two options of rigid body rotation (clockwise and anticlockwise) bring about two physically distinct situations, namely, either one or both twin components satisfy the IPS condition approximately. The corresponding substructures clearly depict the consequence—formation of either a stack of very thin twins or of alternate twins with the thickness ratio of 1:4.

The structure of martensite produced in rapidly solidified pure zirconium and zirconium–niobium alloys

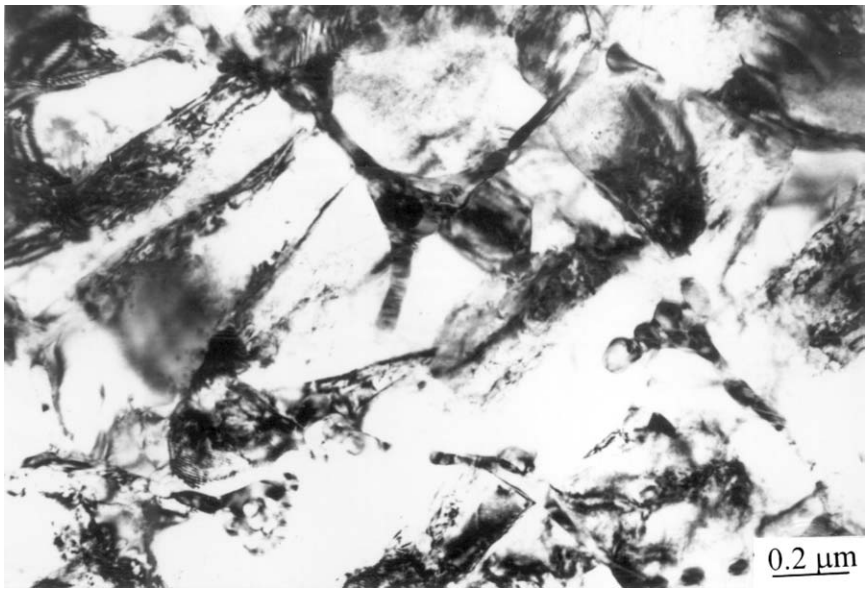


(a)

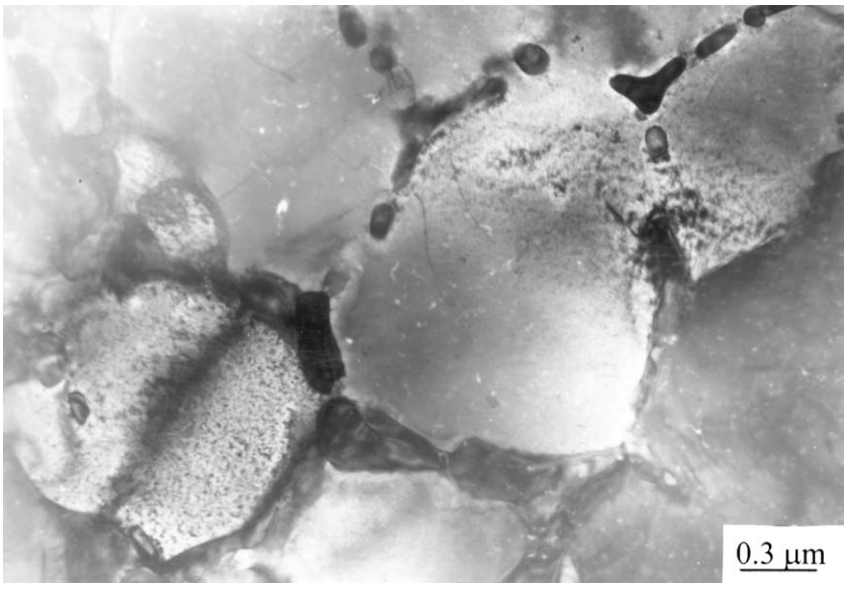


(b)

*Figure 2* (a) Bright-field micrograph showing the formation of the $\beta$ phase from the liquid followed by a martensitic transformation. (b) Bright-field micrograph showing the formation of the $\alpha$ phase directly from the liquid phase.

was reported in the work of Banerjee and Cantor [3], which has revealed the interplay of the solidification structure and the subsequent martensitic transformations. In case of partitionless solidification, the $\beta$ grains inherit the composition of the liquid and these grains remain compositionally homogeneous. Martensite plate once nucleated can, therefore, propagate across the entire parent $\beta$ grains. When cellular morphology of the $\beta$ grains are produced, the composition of the $\beta$ grain changes from the centre of the cells to their peripheries. This variation in composition is associated with a gradual drop in the $M_s$ temperature, as shown in Fig. 4 in the case of Zr-Nb alloys where Nb is a $\beta$ stabilizing element. The growth of the martensite plate nucleated in a $\beta$ cell of varying composition is, therefore, expected to stop when the tip of the plate reaches a point where the $M_s$ temperature is lower than the quenching temperature. Under these circumstances, martensite plates remain confined within the individual cells of the solidification structure.

In case the $M_s$ temperature in the inter cellular region is not depressed below the quenching temperature, the growing martensite plates can cut across inter cellular boundary disregarding the variation in chemical composition in its path. Examples of the latter type of martensitic growth were encountered more frequently in Zr-Nb alloys with Nb level upto about 3% (Fig. 5).

## 4. Competition between two displacive transformations: $\beta \rightarrow \alpha'$ and $\beta \rightarrow \omega$

Zirconium alloys are known to exhibit two distinct displacive transformations—the $\beta \rightarrow \alpha'$ martensitic and $\beta \rightarrow \omega$ transformations [7], the $M_s$ temperatures corresponding to the two processes being depicted in Fig. 4. Martensitic transformation has been described in the

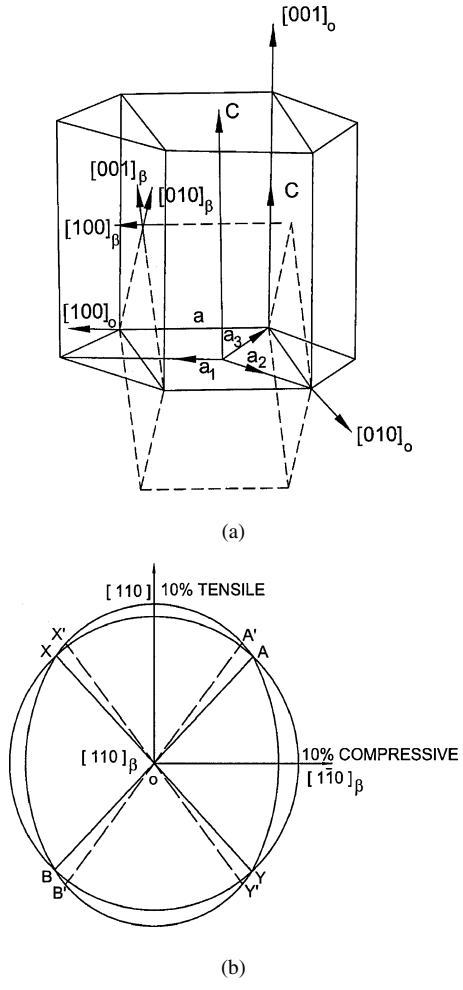


*Figure 3* (a) Lattice correspondence between the $\alpha$ and $\beta$ phases. (b) Strain ellipsoid corresponding to the martensitic transformation in Zr alloys.

previous section while the $\omega$ transformation is discussed below:

The $\omega$ phase, which is an equilibrium phase in Group IVA metals at high pressures, forms in several alloys based on titanium, zirconium and hafnium and also in many other bcc alloys as an athermal transformation product [7].

The mechanism of the $\beta \rightarrow \omega$ transformation can be viewed as a collapse of the (222) lattice planes of the bcc structure in a sequence shown in Fig. 6 . The ABCABC stacking of the (222) planes changes to the AB′AB′ stacking of the basal planes of the $\omega$ phase as B and C planes are collapsed on to the intermediate B′ plane, keeping the A layer unaltered. The periodic displacement of the (222) planes can be represented as a longitudinal displacement wave, where the displacement, $U_p$, of the $p$th plane is expressed as

$$U_p = A_d \sin K_\omega X_p$$

$A_d$ being the amplitude and $K_\omega$ the wave vector ($= 2\pi/3d_{222}$) of the displacement wave and $X_p$ ($= pd_{222}$) being the distance of the $p$th (222) plane from the origin. The athermal $\beta \rightarrow \omega$ transition is associated with the following characteristic features: (1) the appearance of an extensive diffuse intensity distribution with the maximum intensity located close to the ideal $\omega$ reflections, as a precursor to the transformation event; (2) the occurrence of a pronounced dip in the $\langle \xi\xi\xi \rangle$ longitudinal phonon dispersion curves in the $\omega$-forming systems at a position slightly away from that corresponding to ideal $\omega$ ($\xi = 0.667$); and (3) the stability of the dual-phase $\beta + \omega$ structure with extremely fine (1-2 nm) $\omega$ particles distributed in the $\beta$ matrix along $\langle 111 \rangle_\beta$ directions. In order to account for these characteristic features, Cook [8] has invoked a modulated $\omega$ structure associated with a wave vector $K_m$ which is close to but slightly larger than $K_\omega$. The modulation arises owing to the difference $K_m - K_\omega (= q)$ and the resulting long period structure, which consists of $\omega$ wave packets dispersed in the $\beta$ matrix, is associated with a lower free energy than the ideal $\omega$ structure.

Both the $\beta \rightarrow \alpha'$ and the $\beta \rightarrow \omega$ transformations are associated with start temperatures as $M_s(\alpha')$ and $M_s(\omega)$, the temperature dependence of which are shown in Fig. 4. As can be seen from this figure, $M_s(\omega)$ is encountered first while quenching in alloys with Nb content exceeding 7%. Therefore, in alloys containing upto about

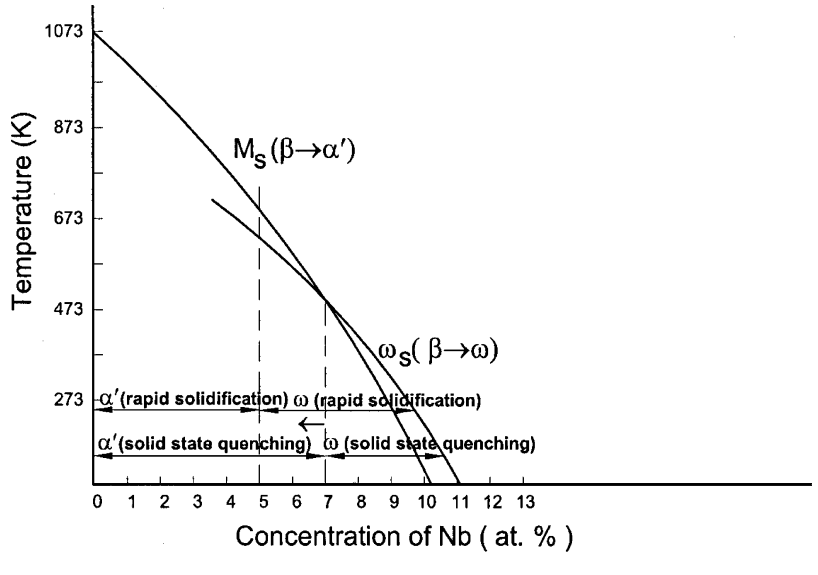


*Figure 4* Variation of $M_s$ and $\omega_s$ temperatures with Nb content in case of Zr-Nb alloys.

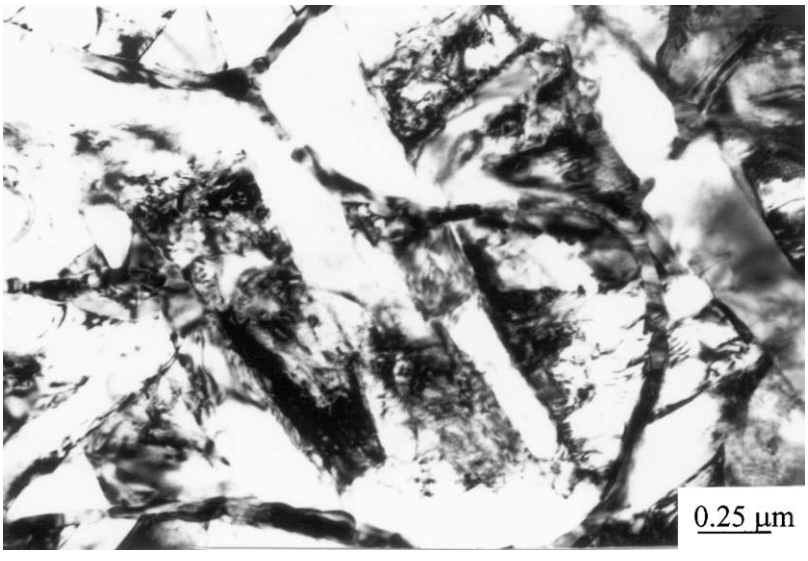


*Figure 5* Bright-field micrograph showing martensitic structure cutting across the cellular boundaries.

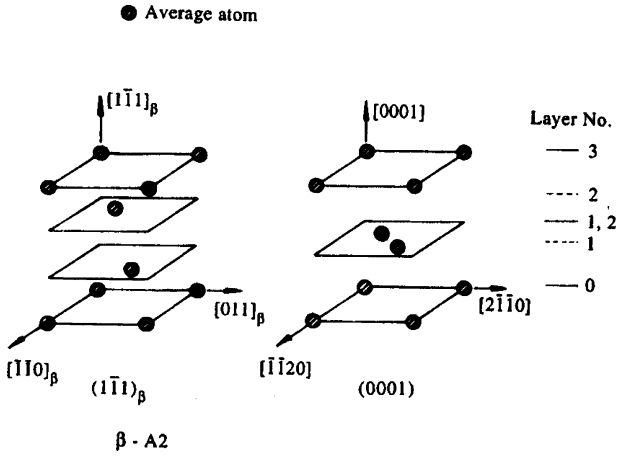


*Figure 6* Lattice correspondence between the $\beta$ and $\omega$ structures. Positions 0, 1, 2 and 3 represent layers A, B, C and A respectively. The position in-between 1 and 2 which has been denoted as 1, 2 represents layer B′.

7% Nb quenching produces $\alpha'$ martensite whereas in those with Nb content higher than 7% the $\beta \rightarrow \omega$ transformation occurs on quenching from the solid state. In rapidly solidified samples, it was observed (Fig. 7) that this transition from the $\beta \rightarrow \alpha'$ to the $\beta \rightarrow \omega$ is shifted to a position close to about 5% (Fig. 4). Fig. 7 is a dark field micrograph showing the formation of $\omega$ phase in Zr-5% Nb alloy. This observation has been attributed to a higher concentration of vacancies in rapidly solidified samples. Vacancies are known to stabilize $\omega$-like defects, which can promote the $\beta \rightarrow \omega$ transformations in preference to the $\beta \rightarrow \alpha'$ transformations in alloys containing Nb higher than 5% [2].

## 5. Chemical ordering of the $\omega$ phase in rapidly solidified Zr-Al and Zr-Al-Nb alloys

Banerjee and Cahn [9] reported the occurrence of the $\beta \rightarrow$ $B8_2$ transition in a rapidly solidified Zr-27 at.% Al alloy which underwent a spinodal decomposition prior to ordering. Since the as-quenched structure was an already decomposed structure (Fig. 8), it was not possible to follow the transformation process starting from a homogeneous supersaturated solid solution. The rapid solidification structure of $Zr_3Al$, more recently investigated by X-ray diffraction, has shown presence of a retained $\beta$ structure which, on mechanical grinding, has been seen to amorphize rather easily. A detailed investigation by means of TEM on two samples (A and B) of melt-spun $Zr_3Al$, supplied by S. Gialanella, has revealed the following features. Sample A has solidified into a supersaturated $\beta$ phase, which does not show any sign of decomposition in the as-quenched state. A layer of an amorphous phase has also been detected on this sample**.** Sample B, apparently quenched at a slower rate, shows a modulated structure (Fig. 9) with a distribution of fine, ordered $\omega$ particles. This sample shows a structure remarkably similar to that observed by Banerjee and Cahn [9].

Sample A was aged at different temperatures to examine the steps in the structural evolution. The initial spinodal decomposition, followed by the formation of $B8_2$ particles in the aluminium-enriched regions, could be detected in this sample. Fig. 9 shows the $\langle 100 \rangle$ spinodally modulated structure and the corresponding asymmetric side bands in the diffraction patterns could be seen in Fig. 9. The presence of $B8_2$ superlattice reflections confirmed that the ordered phase has a $B8_2$structure. The transformation sequence during rapid solidification and subsequent cooling or ageing has been found to consist of the following steps, consistent with those reported earlier:

1. Solidification into the supersaturated $\beta$ phase through a partitionless solidification process.
2. Spinodal decomposition of the $\beta$ phase, resulting in a $\langle 100 \rangle$ modulated structure.
3. Formation of $Zr_2Al$ particles, a single particle forming within each cuboidal-shaped aluminium-enriched region.
4. Athermal $\beta \rightarrow \omega$ transformation in the aluminium-depleted regions, resulting in a $(\beta + \omega)$ structure.
5. Transformation of the metastable $(\beta + \omega)$ regions into the equilibrium $\alpha$ phase on ageing.

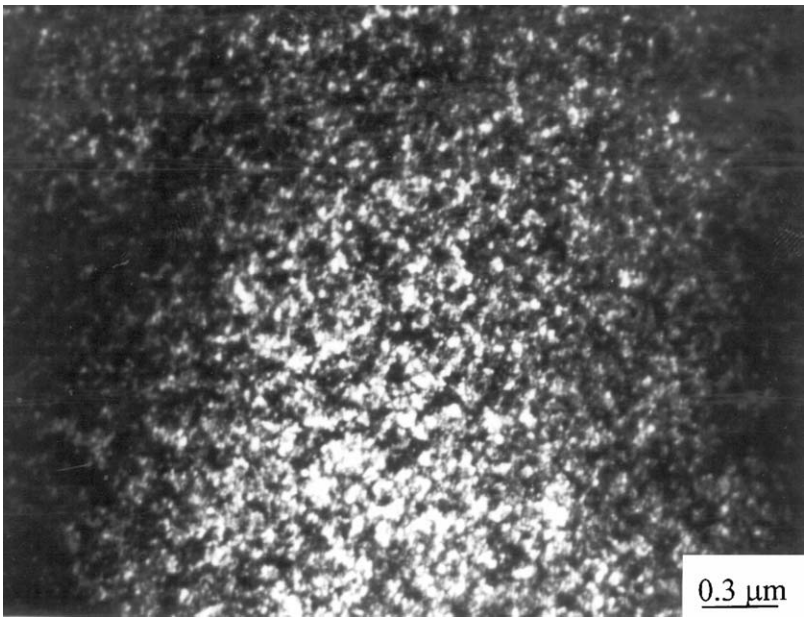


*Figure 7* Dark-field micrograph showing $\omega$ particles in rapidly solidified Zr-5Nb alloy.

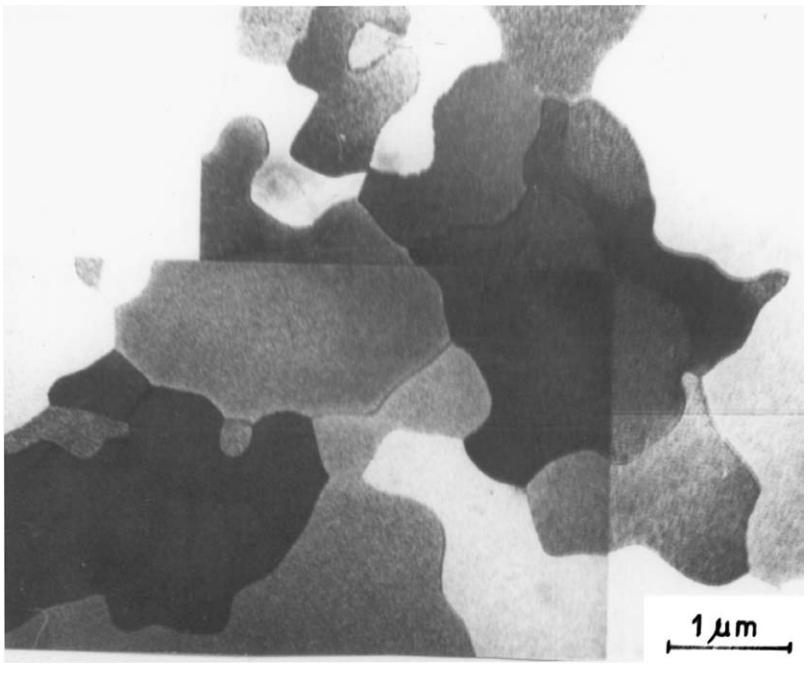


(a)

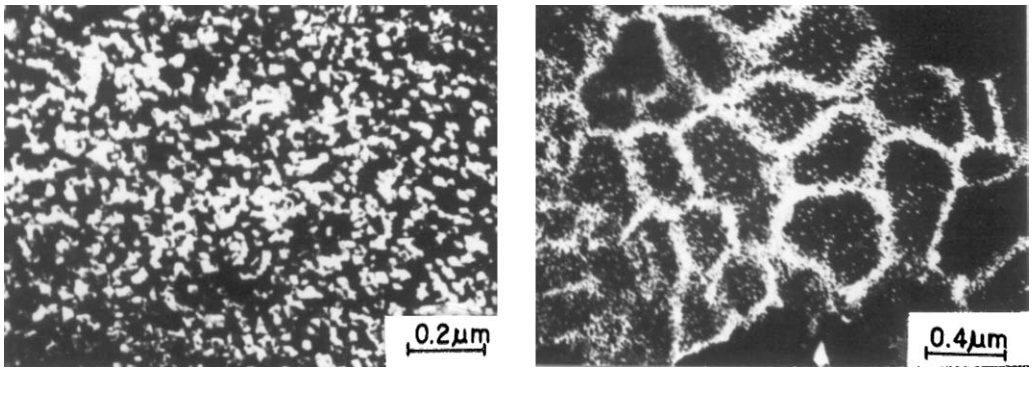


(b) (c)

*Figure 8* Bright-field micrograph of Zr-27 at.%Al alloy showing undulated boundaries characteristic of solidification morphology and a mottled contrast of the matrix resulting from fine scale $Zr_2Al$ precipitates; (b) Homogeneous distribution of $Zr_2Al$ particles as revealed from dark-field images taken with a $Zr_2Al$ reflection (c) Cellular structure leading to Al enrichment at cell boundaries where higher density of $Zr_2Al$ particles are seen.

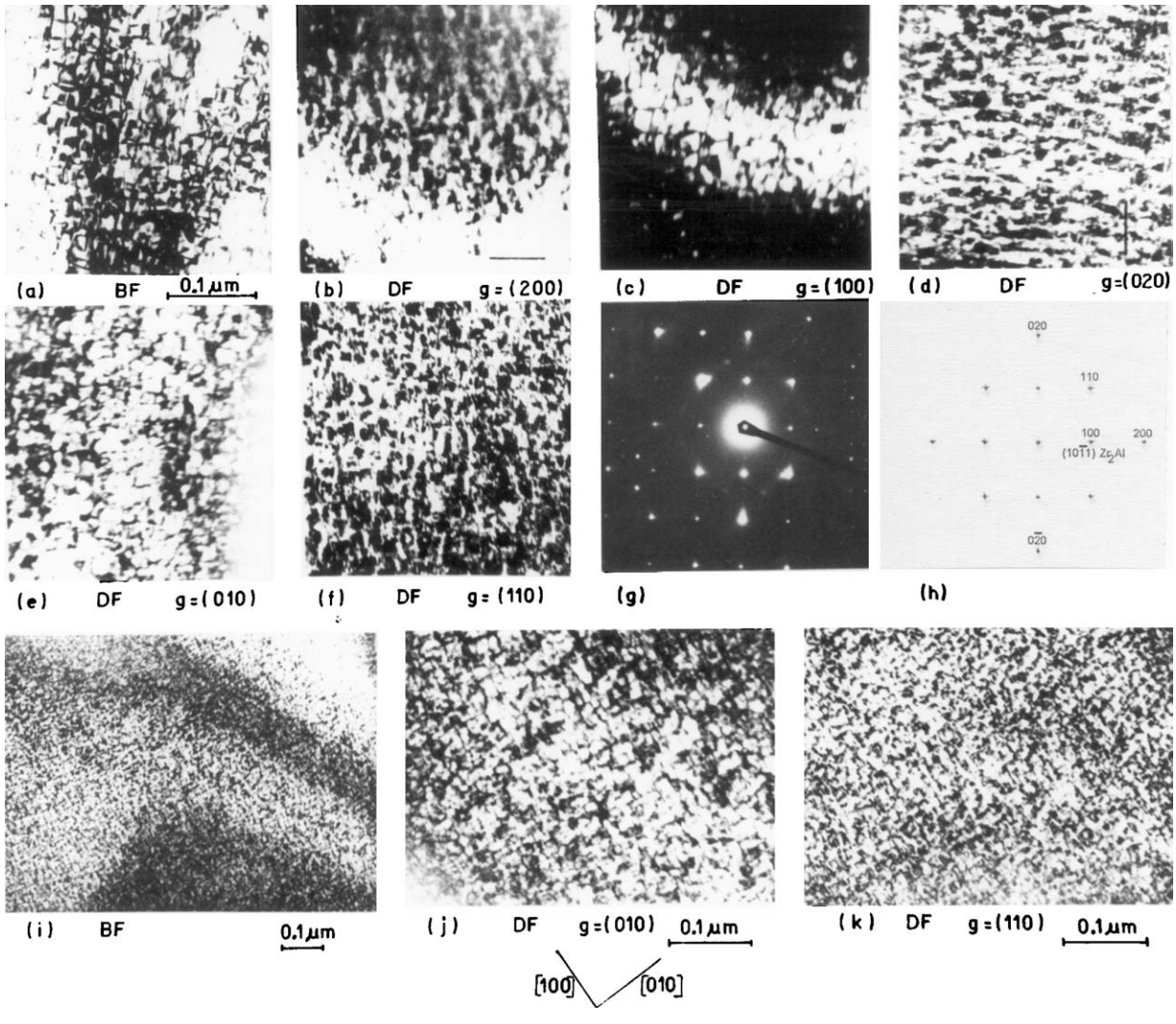


*Figure 9* (a) Bright-field electron micrograph showing $Zr_2Al$ particles. Contrast revealed under different operating reflections, g. Dark-field images with matrix reflections $\langle 200\rangle_\beta$ exhibit $\{100\}_\beta$ striations perpendicular to g ((b) and (d)) while striations along both $\{100\}_\beta$ planes are seen under $(110)_\beta$ reflection (f). Dark-field images of the same area with $\langle 10\bar{1}1\rangle_{Zr_2Al}$ reflections (coinciding with $\langle 100\rangle_\beta$ positions) bring $Zr_2Al$ particles in bright contrast, ((c) and (e)). Contrast variation under different operating reflections and the alignment of $Zr_2Al$ particles along $\{100\}_\beta$ planes are more clearly demonstrated in the set of micrographs (h), (i) and (j).

The lattice correspondence between the bcc and the $B8_2$ structures, as shown in Fig. 10 clearly, indicates that the $\beta \rightarrow B8_2$ transition can be viewed as a superimposition of periodic displacements and a concentration wave on the bcc structure. The displacement wave (identical to that corresponding to $\beta \rightarrow \omega$) and the concentration waves that can accomplish the transition are shown in Fig. 11**.** In contrast with the fine particle morphology of athermal $\omega$ particles that remain aligned along $\langle 111\rangle$ directions in the dual-phase $\beta + \omega$ structure, the $Zr_2Al$ particles have been found to be of a fairly large size (about 20 nm). Cuboid-shaped aluminium-rich regions form at the nodes of the three-dimensional $\langle 100\rangle$ concentration waves. These aluminium-rich regions finally transform into a single $Zr_2Al$ particle. The fact that within each of these cuboids neither all possible variants are nucleated nor a dual-phase structure is formed suggests that the transition occurs homogeneously and not by a nucleation and growth process. This is quite likely in view of the large supercooling provided in the present case where the $M_s(\omega)$ temperature is as high as about 1300 K.

Having observed the displacive/replacive $\beta \rightarrow B8_2$ transition in rapidly solidified binary alloys close to the $Zr_3Al$ composition, an attempt has been made to stabilize the $\beta$ phase by introducing a ternary element, niobium. The rapidly solidified structures of $(Zr_3Al)$-3% Nb and $(Zr_3Al)$-10% Nb show a distribution of ordered particles in a $\beta$ matrix (Fig. 12a). SAD patterns from the ordered phase in these alloys, though remarkably similar to those associated with the $B8_2$ structure for most of the zone axes, were found to be consistent with $D8_8$structure, which is the reported structure of the equilibrium $Zr_5Al_3$ phase. On the basis of the observed orientation relationship between the $\beta$ and the $D8_8$ structures and their lattice dimensions, the lattice correspondence between the B2 and the $D8_8$ structures has been determined (Fig. 12b). It is clear from this correspondence that the $\beta \rightarrow D8_8$ transition can also be described in terms of a combination of displacive and replacive ordering. Omega-like displacement modulations can generate the right sequence of atomic layers. Suitable chemical ordering superimposed on this can produce the $D8_8$ structure. It must be emphasized here

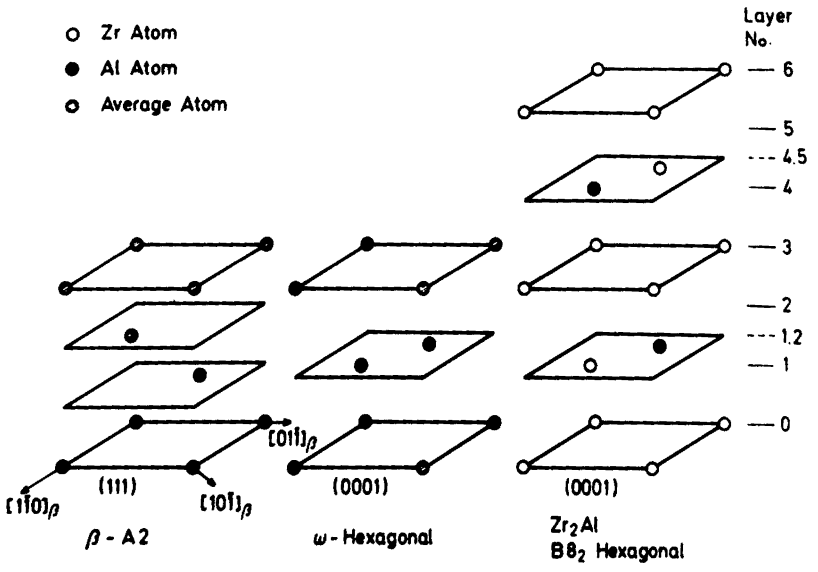


*Figure 10* Lattice correspondence between the bcc and the $B8_2$ structures.

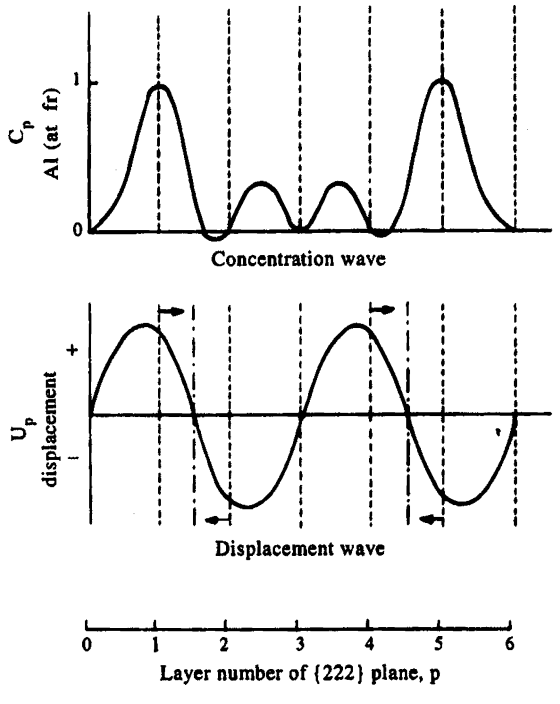


*Figure 11* Periodic displacement and concentration waves corresponding to the $\beta \rightarrow B8_2$ transition.

that the $D8_8$ structure is a vacancy ordered structure, which has 16 atoms per unit cell as against the 18 atoms of the bcc structure that are involved in producing the $D8_8$ structure. The ease of retention of high vacancy concentrations in the bcc structure on quenching from the liquid state and the thermodynamic stability of vacancies in vacancy ordered structures like $D8_8$ appear to be responsible for including the $\beta \rightarrow D8_8$ transition during rapid quenching from the liquid state.

## 6. Glass formation in Zr based alloys

Zr-based alloys have been obtained in the glassy state by rapid solidification as well as by bulk glass forming techniques. Identification of factors that determine whether a particular alloy can be obtained in the form of rapidly solidified metallic glasses or bulk metallic glasses, though quite important, is not very easy. There is no single key parameter, that can alone describe glass-forming ability (GFA) [10], since numerous factors have been found to influence GFA. Thermodynamically, glass formation is favoured within certain composition ranges of some systems where the free energy difference between the supercooled liquid and the metastable and stable phases competing with glass formation is as small as possible [10]. Similarly, there are approaches based on kinetic factors, size and electron theory considerations. The free energy of the liquid phase and that of the intermetallic compounds can be established by determining the free energy of different phases as a function of composition in binary alloy systems. This is possible by a thermodynamic analysis of the phase diagram incorporating some experimental thermodynamic data [11]. From the free energy hierarchy of several competing phases it could be observed that in the Zr-Ni system, the driving force for crystal formation in Zr-rich alloys was much smaller in case of $Zr_{67}Ni_{33}$ as compared with that of the $Zr_{76}Ni_{24}$ alloy [11]. This observation was indicative of the fact that thermodynamically glass formation tendency was greater at compositions close to that of the first intermetallic compound and not the first eutectic composition. The Zr transition metal-metal systems provide opportunities for comparing the glass forming ability of the eutectic compositions such as $Zr_{76}Ni_{24}$ and of intermetallic compounds such as $Zr_{76}Fe_{24}$. The eutectics, though considered better glass formers, can in fact have a poorer glass forming ability due to the presence of metastable phases competing with glass formation or low viscosity of the melt at the eutectic composition due to lack of ordering in the melt. On the other hand, glass formation in the intermetallic compounds may be favoured because of the higher viscosity of the melt due to ordering in the liquid phase or due to slow nucleation of the intermetallic compounds because of their complex structure. This conclusion has been arrived at by

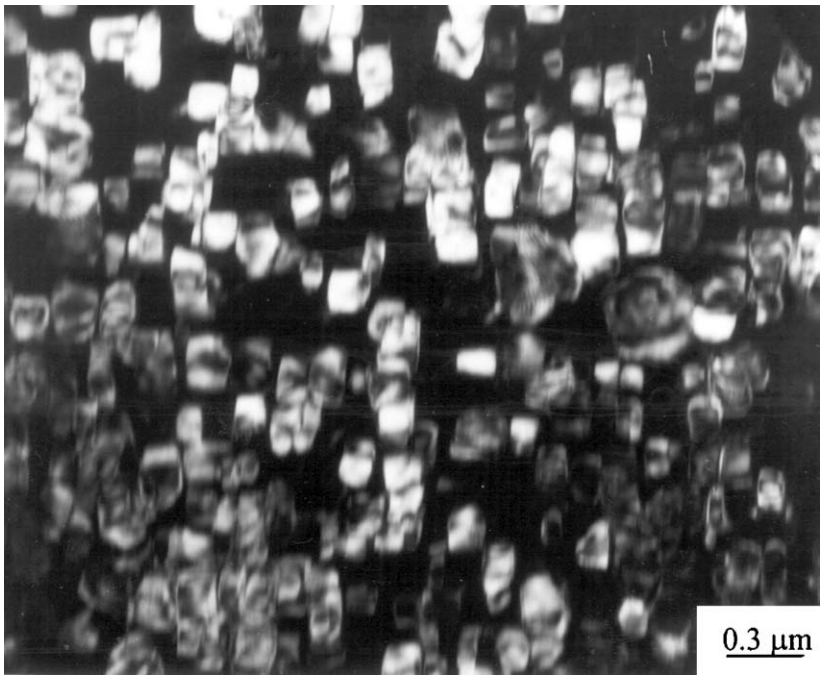


(a)

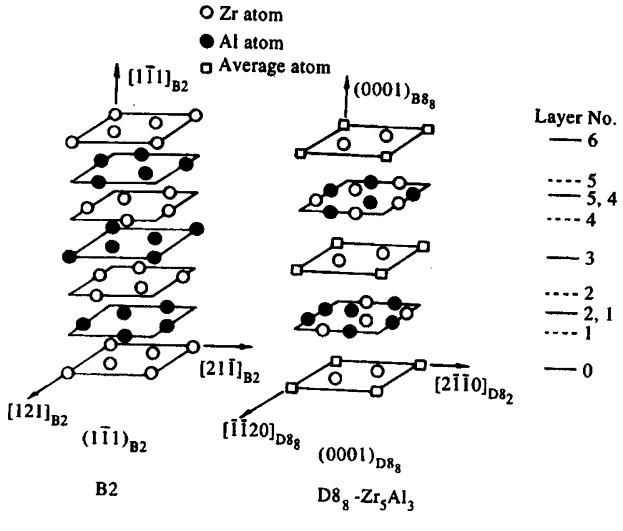


(b)

*Figure 12* (a) Bright-field micrograph showing the distribution of ordered $\omega$ particles in a $\beta$ matrix. (b) Lattice correspondence between the $\beta$ and the $D8_8$ structures.

considering the kinetic factors as well and is elaborated on later.

Another approach based on thermodynamics is the concept of the $T_o$ curve [12, 13]. The $T_o$ curve in the phase diagram is the locus of compositions at each temperature, where the liquid and the solid phases of the same composition have the same value of the molar free energy. The position of the $T_o$ line in the phase diagram should be known in order to make predictions about the formation of a single solid solution after rapid solidification for a given alloy system. Based on the position of $T_o$ curves in the phase diagram, Dey *et al.* [14] and Boettinger *et al.* [15] have examined the conditions for partitionless solidification. In composition ranges where the $T_o$ temperature is depressed, it has been suggested that glass formation is easier. In alloys having low $T_o$, if rapid solidification can suppress alloy partitioning, the liquid can be undercooled to such an extent that it can be vitrified. The position of the $T_o$ line in the Zr-Ni system has been established by an approach suggested by Katgerman [16] and it could be seen that $T_o$ drops rapidly with increasing Ni content (Fig. 13), indicating that exceptionally large undercoolings will be required for formation of $\beta$ phase of the same composition as the liquid in hypereutectic compositions, a factor which will favour glass formation in these compositions.

During glass formation, the destabilization of the crystalline phase rather than the stabilization of the glass phase is important [17]. By supercooling a liquid in such a way that crystal nucleation and growth is avoided, glass can be obtained in any liquid. The avoidance of crystal formation approach has been found to be the most appropriate, out of the several approaches

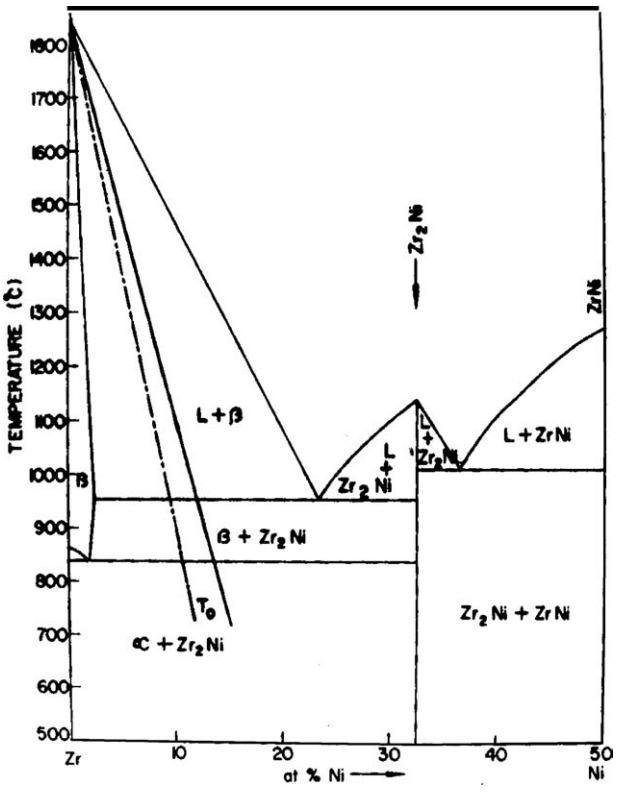


*Figure 13* The liquid/$\beta T_0$ lines drawn on the zirconium rich side of the Zr-Ni phase diagram. Firm line—regular solution. Dotted line—ideal solution.

suggested for evaluation of the glass forming ability of the alloys. Crystal nucleation and growth kinetics are considered separately in this approach. From the crystal nucleation point of view, the conditions under which a "glass" can form are: (i) complete suppression of nucleation, (ii) limited nucleation of crystals but no significant growth of these, and (iii) nucleation of a very few isolated crystals followed by their substantial growth while the major part of the matrix vitrifies. The quenched product can be qualified to be an amorphous material if the volume fraction of the crystalline phases present is negligibly small. Condition (i) is difficult to achieve during a process like melt spinning. Condition (ii) leads to the formation of quenched-in nuclei, which do not get an opportunity to grow. This condition is most readily satisfied during melt spinning in the case of Zr-based glass forming alloys. Consequently, the amorphous matrix usually contains a distribution of quenched-in-nuclei, their density being controlled by the rate of nucleation during the cooling down path. Though transient nucleation times are of the order of microseconds, for rapid quenching such short transient times are significant, because these are a good fraction of the total solidification time [18, 19]. Savalia *et al.* [20] have calculated the transient nucleation times in the case of Zr-based ternary glasses based on an approach suggested by Kelton *et al.* [18, 19]. The quenched-in-nuclei are very small in size and volume fraction and hence are very difficult to detect. High-resolution electron microscopy can be used to determine the structure of these as has been done by Savalia *et al.* [20]. These nuclei mostly form in the transient nucleation stage before the attainment of the steady state nucleation rate [18, 19]. Savalia *et al.* [20] have also calculated the steady state nucleation frequency using the equation proposed by Turmbull [21] and have found it to be much higher in Zr-based alloys as compared with that in a very good glass forming system like Pd-Si [20, 22–24]. In Zr-based alloys amenable to glass formation by rapid solidification, therefore, glass formation is possible only if homogeneous nucleation is avoided. However, in bulk glass forming Zr-based alloys the role of heterogeneous nucleation acquires a greater significance. This aspect will be discussed later. Condition (iii) leads to the formation of a few large crystals in a matrix of the amorphous phase, the crystalline particles being few and far between. A study of the microstructure of these partially crystalline materials yields information regarding the identity of the crystalline phase competing with glass formation, their formation mechanism from the liquid phase, and estimation of the quantity of the crystalline phase gives the glass forming ability of the alloy.

Easy glass formation not only requires slow nucleation but also needs slow growth of crystals, which may be slow due to either need for partitioning of solutes or due to the need for chemical ordering in the growing phase. The interface temperature of a crystal growing in a undercooled melt has been calculated by Savalia *et al.* [20] using the one-dimensional model for crystal growth developed by Greer and Evans [25]. Their calculations have shown that for a ternary Zr-based alloy $Zr_{76}Fe_{16}Ni_8$, for a very small superheat the interface temperature drops below $T_g$ before the liquid to crystal transformation is complete, indicating easy glass formation in this alloy. The relative glass forming ability of some alloys in the Zr-Ni system has been determined by estimating the amount of crystalline phase in the partially crystalline alloys [26]. The morphology of the crystals in the partially crystalline alloys has been examined by Dey and Banerjee [27] and Tanner [28]. The former authors encountered single crystals (Fig. l4a) and crystal aggregates (Fig. l4b) embedded in the amorphous matrix. A very interesting sunflower-like morphology (Fig. l4b) arising out of twin-relation between the adjacent crystals could be seen in some of these aggregates. Depending upon the local conditions of solidification, different types of crystal/amorphous interfaces were encountered [20, 27].

In many of these studies, estimates of the nucleation frequencies and that of the growth rate have been made using the free energy difference between the crystalline phase and that of the liquid phase at different levels of undercooling. This quantity can be estimated by various methods. Savalia *et al.* [20] were the first to make an attempt to evaluate this quantity from experimentally determined parameters. Their approach has been elaborated in ref. [11]. The overall crystal formation kinetics can be evaluated in terms of classical phase transformation kinetics theory and represented as isothermal time-temperature-transformation (TTT) diagrams. Such diagrams were first developed by Ulhman [29] and subsequently used by Davies [30] to determine the value of the critical cooling rate to just

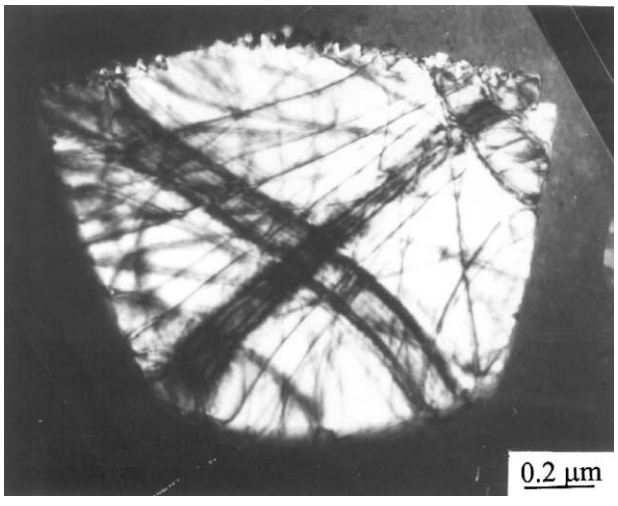


(a)

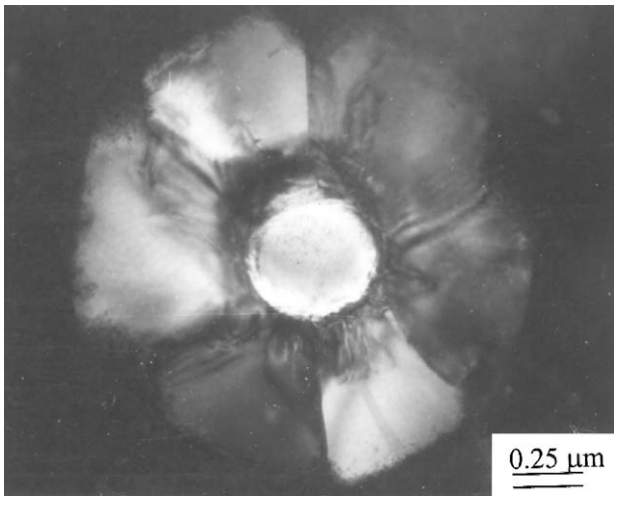


(b)

*Figure 14* (a) Bright-field electron micrograph showing a single crystal and (b) an aggregate of crystals embedded in amorphous matrix of Zr based glass.

avoid crystallization. Savalia *et al.* [20] have used this approach and the $\Delta G_c$ calculated from experimentally determined parameters for estimating the critical cooling rate for glass formation in the case of $Zr_{76}Fe_{16}Ni_8$ and found it to be close to $10^6$ K/min. This value is in good agreement with that for other alloys in this system [20]. The TTT diagrams for two Zr-Ni alloys, $Zr_{67}Ni_{33}$ and $Zr_{76}Ni_{24}$ were constructed by Dey [31]. It could be seen from these diagrams that the critical cooling rate for glass formation was lower for the $Zr_{76}Ni_{33}$ alloy as compared with the $Zr_{76}Ni_{24}$ alloy, though the latter is the eutectic composition. This estimation clearly demonstrated that the eutectic composition need not necessarily be the composition at which glass formation is the easiest. The factors of importance are the viscosity of the melt and the free energy difference between the liquid and solid phases.

The formation of bulk metallic glasses can also be based on certain criteria. According to Liu *et al.* [32], the important points which need to noted for bulk metallic glass formation are: (a) multicomponent systems consisting of more than three elements, (b) large atomic size ratios above 12 pct among the constituent elements, and (c) negative heats of mixing among the elements. These are thermodynamic criteria. There are some kinetic criteria also. The foremost requirement is the avoidance of crystallization. Bulk glass formation occurs when crystal nucleation and growth can be avoided even at low cooling rates. Besides other factors, diffusivity in the melt is one important factor controlling the kinetics of crystal nucleation and growth in the under cooled melt. In ceramic and organic systems where bulk glass formation is very easy, melt viscosities below melting point has been found to be very high [33]. In metallic systems as well, the formation of bulk metallic glass would be easy if the melt viscosities are high. A large number of Zr-based alloys have been obtained in the bulk amorphous state [37]. It appears that not only are the melt viscosities high for these alloys, $\Delta G_c$ the free energy difference between the liquid and the crystalline phase competing with glass formation, is also low. The lower values of $\Delta G_c$ in the case of Zr based ternary Fe-and Ni-bearing glasses as compared with other estimates has been indicated in the study carried out by Savalia *et al.* [20]. Threat to glass formation in case of bulk glass forming alloys is not from homogeneous nucleation, because homogeneous nucleation frequencies are low in such alloys. Heterogeneous nucleation of crystals is likely to pose a more serious challenge to glass formation in such alloys, and it is necessary to completely eliminate or minimize heterogeneous nucleation sites in these alloys in order to get bulk glass. A very large number of Zr-based alloys have been obtained in the glassy state in bulk and many of these are listed in ref. [34].

## 7. Crystallization of Zr-based metallic glasses

Zr-based metallic glasses show a variety of crystallization modes that have been studied in detail in Zr-Cu, Zr-Cr, Zr-Be, Zr-Ni and Zr-Fe systems [35–40]. Primary, eutectic and polymorphic crystallization reactions have been encountered in these glasses. Studies in Zr-based ternary glasses are fewer in comparison. The overall crystallization kinetics has been studied in a number of Zr-based binary alloys by differential scanning calorimetry (DSC) [27, 38, 39]. The activation energy of crystallization has been determined by the Kissinger peak shift method in the case of Zr-Ni, Zr-Fe and Zr-Fe-Ni alloys [38–40]. Dey *et al.* [ 27, 40–42] have studied the crystal nucleation and growth kinetics separately by TEM in case of $Zr_{67}Ni_{33}$ and $Zr_{76}Fe_{24}$ glasses which undergo polymorphic crystallization leading to the formation of $Zr_2Ni$ and $Zr_3Fe$ phases, respectively. Dey *et al.* [39] have found that the nucleation density increased with time linearly at all temperatures. They found that the growth rate of the crystals was constant at each temperature for the alloys showing polymorphic crystallization [39]. The $Zr_{76}Ni_{24}$ glass undergoes eutectic crystallization leading to the formation of the $\alpha$?(hcp) and the $Zr_2Ni$ (bct) phases. A continuous substitution of Fe by Ni is not expected in these intermetallic phases during the crystallization of amorphous alloys containing progressively increasing amounts of Ni, since the

equilibrium $Zr_3Fe$ and $Zr_2Ni$ phases are not isostructural. $Zr_3Fe$ phases has a base—centered orthorhombic (bco) structure. Dey *et al.* [39] in their study of crystallization of Zr-based ternary glasses containing Fe and Ni have attempted to address the following questions: (a) How the addition of the third alloying element effects the process of crystallization? (b) Whether any new phases form in these alloys during crystallization? and (c) To what extent Fe and Ni can be mutually substituted in the intermetallic compounds $Zr_3Fe$ and $Zr_2Ni$? It was observed by Dey *et al.* [39] that addition of Ni to the Zr-Fe alloys reduces the thermal stability of these glasses. These authors have shown [39] that in compositions where surface crystallization occurs, the crystallization temperature drops substantially.

Crystallization of rapidly solidified as well as bulk metallic glasses can also lead to the formation of nanocrystalline structures. In the Zr-based ternary alloys having compositions $Zr_{76}Fe_{24-x}Ni_x$ where $x <$ 12, Dey *et al.* [39] have shown that nanocrystal formation can occur under suitable conditions of crystallization. The requirement for the formation of the nanocrystalline structures is that a large number density of nuclei should form and these nuclei should grow to the stage of impingement without leaving any untransformed amorphous matrix and this can be realized if the rate of steady state nucleation of crystals is high. Though crystallization of rapidly solidified as well as bulk glass can lead to the formation of nanocrystalline structures, there is a subtle difference. The formation of nanocrystals occurs only in glasses having certain compositions, because the steady state nucleation rates of crystals are high in these glasses. The formation of nanocrystals during crystallization in the case of rapidly solidified metallic glasses is expected in view of the fact that these are alloys where the steady state homogeneous nucleation rate is high. This is why these compositions require rapid solidification to prevent homogeneous nucleation and facilitate glass formation. In case of bulk metallic glass forming alloys, the homogeneous nucleation frequencies are low compared with those compositions where glass formation requires rapid solidification. Threat to glass formation in such alloys is not from homogeneous nucleation, and bulk metallic glasses can be obtained in these alloys at low cooling rates provided heterogeneous nucleation has been avoided. Though the homogeneous nucleation frequency is low in bulk glass forming alloys, formation of nanocrystalline phases has been noticed in many bulk glasses after crystallization. In this regard, it is interesting to compare the nanocrystal formation behaviour of the bulk glass and the rapidly solidified Zr-based glasses. The size of the nanocrystals can be made very fine by suitable heat treatment in the rapidly solidified metallic glass, whereas in bulk glass the crystal size could not be made very small. This difference in size can be traced to the fact that in case of bulk glass the homogeneous nucleation frequency is low, which leads to less copious nucleation of crystals as compared to rapidly solidified metallic glass.

Dey *et al.* [43] have examined the nanocrystals formed by crystallization of $Zr_{52}Ti_6Al_{10}Cu_{18}Ni_{14}$bulk metallic glasses using HREM (Fig. 15). The emphasis of their studies has been in examining the structure of the nanograin boundary and other types of defects in the nanograins. The structure of the nanograin boundary has been examined by HREM in the case of many elements like Cu and Pd in the nanocrystalline state [44–46]. It could be seen in images examined by Dey *et al.* [43] that the lattice fringes progressed from one end


*Figure 15* HREM micrograph showing nanocrystal in crystallized bulk metallic glass.

of the grain to the other and extending almost up to the grain boundary. In some of the grains, a slight change in contrast of the lattice fringes near the nanograin boundary could be seen. This was mostly manifested in the form of distortion and curving of the fringes. It was possible to see a region along the grain boundary having a different contrast. This region was localized to a distance of about 0.5 nm. However, all the aforementioned features were also encountered in images of grain boundaries obtained from large-grained material. In this regard, the observations are very similar to those made by Thomas *et al.* [46] in case of nanocrystalline Pd where no manifestation of grain boundary structures with random displacements of average magnitude greater than 12% of nearest neighbour distance could be observed. The nanograin boundary was found to be a large angle grain boundary in most cases and no coherency could be encountered between the planes along any orientation. It was not possible to see the presence of voids at any of the nanograin boundaries examined. Dislocations were observed in the specimen, though their number density was quite small. In some of the grains, it was also possible to see features similar to stacking faults and antiphase domain boundaries [47]. The ordered intermetallic compound phases, like the ones examined in such studies [43, 48], provide an opportunity to study interfaces like these because these will not be readily encountered in pure elemental nanocrystalline materials. The images of the antiphase boundary observed in this study were compared with those encountered in large grains of similar phases, and structurally was observed to be very similar. The stacking faults encountered in this study resembled those seen in the case of phases having similar structure and large grains [47].

Twins could be seen in many of the nanograins examined in studies carried out by Dey *et al.* [43]. The structure of the twins in nanocrystals was found to be identical to that seen in the case of large-grained materials. However, the propensity of these twins was found to be much larger. This observation is in keeping with that made in the case of studies carried out in many other nanocrystalline solids where extensive twinning has been found to occur [49, 50]. The presence of twins in the nano-crystalline phases is most probably due to the fact that the stress in the small grains is too large because of their size and the growth of the nanograins necessitates the formation of twins.

## 8. Zr-based quasicrystalline phases

A large number of alloy systems have now been identified where the quasicrystalline phase can be obtained by crystallization of an amorphous phase. Many of these alloys are Zr-based, and important alloys systems where quasicrystalline phases have been found are Zr-Pd [51], Zr-Ni-Ti [52] and other Ti/Zr-TM [53] alloys besides multicomponent Zr-Cu-Ni-Al alloys [54]. Of these alloys, $Zr_{69.5}Cu_{12}Ni_{11}Al_{7.5}$, an alloy in the last mentioned system, is now very well known for its quasicrystal formation tendency after rapid solidification and crystallization, and has also received considerable attention by way of studies pertaining to hydrogen storage. In this alloy and many other alloys, crystallization has led to the formation of a nanoquasicrystalline solid. Savalia *et al.* [55] have examined the structure of the nanograin boundary in the case of this alloy and shown that there are many similarities in structure of these boundaries with those of grain boundaries in solids having large quasicrytsalline grains. It has been proposed that many of these alloys have icosahedral short range order in their undercooled melts and amorphous phases [56].

## 9. Conclusions

This review highlights the variety of phase transformations that are possible in melt-quenched Zr-based alloys. These include direct liquid → alpha transformation, liquid → beta → martensitic transformation and transformation of liquid → beta → ordered omega phases, besides the liquid → glass and liquid → nanocrystal transformation shown by many Zr-based alloys. Zr-based alloys have also shown liquid → quasicrystal and liquid → amorphous → quasicrystal transformation. The various studies on zirconium-base metallic glasses have made important contributions towards a better understanding of several issues connected with amorphous alloys. The glass forming ability of Zr based alloys can be rationalized on the basis of the thermodynamic stability of the liquid phase and the kinetic consideration of avoidance of a competing crystalline phase under a given condition of cooling. Crystallization of rapidly solidified and bulk Zr-based metallic glasses can lead to the formation of nanocrystalline phases. In case of quasicrystal forming alloys, formation of nanoqausicrystals has also been encountered.

## References


1. S. BANERJEE and P. MUKHOPADHYAY, "Phase Transformation: Examples from Titanium and Zirconium Based Alloys, Pergamon Series in Materials Science, Series," edited by R. W. Cahn, Elsevier.
2. ISHAN BARIN, "Thermochemical Data of Pure Substances," 3rd ed., Vol. II, (VCH Publisher, 1995) p. 1851.
3. S. BANERJEE and B. CANTOR, "Int. Conf. on Martensite" (MIT Press, Boston, 1979) p. 195.
4. Y. INOKUTI and B. CANTOR, *J. Mater. Sci.* **12** (1977) 946.
5. F. DUFLOS and B. CANTOR, in Proc. 3rd International Conf. on Rapidly Quenched Metals, *Metal Soc. London*, edited by B. Cantor (1978) Vol. I, p. 110.
6. S. BANERJEE and R. KRISHNAN, *Acta Meter.* **19** (1971) 1317.
7. S. K. SIKKA, Y. K. VOHRA and R. CHIDAMBARAM, *Prog. Mater. Sci.* **27** (1982) 245.
8. H. E. COOK, *Acta Metall.* **23** (1974) 239.
9. S. BANERJEE and R. W. CAHN, *ibid.* **31** (1983) 1721.
10. H. A. DAVIES, in "Amorphous Metallic Alloys" edited by F. E. Luborsky (Butterworths, London, 1983) p. 8.
11. J. CHARLES, J. C. GAACHON and J. HERTZ, *Calphad* **9** (1986) 35.
12. I. L. APTEKAR and D. S. KAMENETSKAYA, *Fiz . Met. Metalloved.* **14** (1962) 358.
13. J. C. BAKER and J. W. CHAN, in "Solidification" (American Society for Metals, Metals Park, Ohio, 1971) p. 23.
14. G. K. DEY, E. G. BABURAJ, S. BANERJEE and P. RAMCHANDRA RAO, "Metallic & Semi Conducting Glass" edited by A. K. Bhatnagar (Key Engg. Materials, Trans. The. Pub, Switzerland, 1987) Vol. II, p. 329.

15. W. J. BOETINGER, in Proc. 4th Int. Conf. on Rapidly Quenched Metals, Sendai 1981, edited by T. Masumoto and K. Suzuki (Japan Institute of Metals, Sendai, 1982) p. 99.
16. L. J. KATGERMAN, *Mater. Sci. Lett.* **2** (1983) 444.
17. H. S. CHEN, *Acta Metall. Mater.* **24** (1976) 153.
18. K. F. KELTON and A. L. GREER, *J. Non-Cryst. Solids* **79** (1986) 295.
19. K. F. KELTON, A. L. GREER and C. V. THOMPSON, *J. Chem. Phys.* **79** (1983) 6261.
20. R. T. SAVALIA, R. TEWARI, G. K. DEY and S. BANERJEE, *Acta Metall. Mater.* **44** (1996) 57.
21. D. TURNBULL, *Contemp. Phys.* **10** (1969) 473.
22. G. GHOSH, M CHANDRASHEKARAN and L DELAEY, *Acta Metall. Mater.* **37** (1991) 929.
23. A. L. GREER, "E.P.R.I. Acta Metall. Mater. Workshop on Amorphous and Semiconductors" (Pergamon Press, San Diego, California, 1985) p. 29.
24. A. J. DREHMAN and A. L. GREER, *Acta Metall. Mater.* **32** (1984) 323.
25. A. L. GREER and P. V. EVANS, *Mater. Sci. Engng. Lett.* **98** (1988) 357.
26. G. K. DEY and S. BANERJEE, in Proc. 5th Int. Conf. on Rapidly Quenched Metals. Wuizburg, 1984, edited by S. Steeb and H. Warlimonts (Amsterdam, North Holland, 1985) Vol. I, p. 67.
27. G. K. DEY and S. BANERJEE, *Mater. Sci. Eng.* **76** (1985c) 127.
28. L. E. TANNER, in Proc. 5th Int. Conf. on Rapidly Quenched Metals. Wuizburg, 1984, edited by S. Steeb and H. Warlimonts (Amsterdam, North Holland, 1985) Vol. I, p. 67.
29. D. R. ULHMANN, *J. Non-Cryst. Solids* **16** (1974) 15.
30. H. A. DAVIES, *Phys. Chem. Glasses* **17** (1976) 159.
31. G. K. DEY, Rapid Solidification of Zirconium Alloys, Ph.D. thesis, Banaras Hindu University, Varanasi, 1988.
32. C. T. LIU, L. HEATHERLY, D. S. EASTON, C. A. CARMICHAEL, J. H. SCHNEIBEL, C. H. CHEN, J. L. WRIGHT, M. H. YOO, J. A. HARTON and A INOUE, *Met. Mat. Trans.* **29** (1998) 1811.
33. H. S. CHEN, *Rep. Prog. Phys.* **43** (1980) 355.
34. A. INOUE, "Bulk Amorphous Alloys Preparation and Fundamental Chraracteristics" (Materials Science Foundations 4, Trans Tech Publications, Switzerland, 1998) p. 38.
35. K. H. J. BUSCHOW, *J. Phys. F. Metal Phys.* **14** (1984) 593.
36. M. HARMELIN, R. CALVAYRAC, A. OVIVY, J. BIGOT, P. BURNIER and M. FAYARD, *J. Non-Cryst. Solids* **61/62** (1984) 931.
37. L. E. TANNER, *Acta Metall. Mater.* **28** (1980) 1805.
38. K. H. J. BUSCHOW, *ibid.* **31** (1983) 155.
39. G. K. DEY, R. T. SAVALIA, E.G. BABURAJ and S. BANERJEE, *J. Mater. Res.* **132** (1988) 504.
40. G. K. DEY, E. G. BABURAJ and S. BANERJEE, *J. Mater. Sci.* **21** (1986) 117.
41. G. K. DEY and S. BANERJEE, *Bull. Mater. Sci.* **156** (1992) 543.
42. G. GHOSH, M. CHANDRASHEKARAN and L. DELAEY, *Acta Metall. Mater.* **37** (1991) 929.
43. G. K. DEY, R. T. SAVALIA, S. NEOGY, D. SRIVASTAVA, R. TEWARI and S. BANERJEE, in Proceedings of Processing and Properties of Structural Nanomaterials, MS&T 2003, Chicago (in press).
44. S. RANGANATHAN, R. DIVAKAR and V. S. RAGHUNATHAN, *Scripta Mater.* (in press).
45. D. H. PING, D. X. LI and H. Q. YE, *J. Mater. Sci. Lett.* **14** (1995) 1536.
46. G. J. THOMAS, R. W. SIEGEL and J. A. EASTMAN, *Scripta Metal.* **24** (1990) 201.
47. D. B. WILLIAMS and C. B. CARTER, "Transmission Electron Microscopy III" (Plenum Press, New York).
48. U. KOSTER, in "Phase Transformations in Crystalline and Amorphous Alloys" edited by B. L. Mordike (Deutsche Gesellschaft fur Metallkunde, Oberussel, 1983) p. 113.
49. C. SURYANRAYANA, *Int. Mater. Rev.* **40** (1995) 41.
50. R. CHANDRA, *et al.*, *Nano Struct. Mater.* **8** (1999) 1171.
51. B. S. MURTY, D. H. PING, K. HONO and A. INOUE, *Acta Mater.* **48** (2000) 3985.
52. J. Y. KIM, E. H. MAJZOUB, P. C. GIBBONS and K. F. KELTON, *Mater. Res. Soc. Symp. Proc.* **553** (1999) 483.
53. K. F. KELTON, *ibid.* **553** (1999) 471.
54. U. KOSTER, J. MEINHARDT, S. ROOS and H. LIEBERTZ, *Appl. Phys. Lett.* **69** (1996) 179.
55. R. T. SAVALIA, G. K. DEY and S. BANERJEE, unpublished work.
56. L. Q. XING, T. C. HUFNAGEL, J. ECKERT, W. LOSER and L. SCHULTZ, *Appl. Phys. Lett.* **77** (2000) 1970.